



Open Research Online

Citation

Evans, P.A.; Kennea, J.A.; Barthelmy, S.D.; Beardmore, A.P.; Burrows, D. N.; Campana, S.; Cenko, S.B.; Gehrels, N.; Giommi, P.; Gronwall, C.; Marshall, F. E.; Malesani, D.; Markwardt, C.B.; Mingo, B.; Nousek, J. A.; O'Brien, P. T.; Osborne, J. P.; Pagani, C.; Page, K.L.; Palmer, D.M.; Perri, M.; Racusin, J. L.; Siegel, M.H.; Sbarufatti, B. and Tagliaferri, G. (2016). Swift follow-up of the Gravitational Wave source GW150914. *Monthly Notices of the Royal Astronomical Society: Letters*, 460 pp. 40–44.

URL

<https://oro.open.ac.uk/62751/>

License

(CC-BY-NC-ND 4.0) Creative Commons: Attribution-Noncommercial-No Derivative Works 4.0

<https://creativecommons.org/licenses/by-nc-nd/4.0/>

Policy

This document has been downloaded from Open Research Online, The Open University's repository of research publications. This version is being made available in accordance with Open Research Online policies available from [Open Research Online \(ORO\) Policies](#)

Versions

If this document is identified as the Author Accepted Manuscript it is the version after peer review but before type setting, copy editing or publisher branding

Swift follow-up of the gravitational wave source GW150914

P. A. Evans,^{1★} J. A. Kennea,² S. D. Barthelmy,³ A. P. Beardmore,¹ D. N. Burrows,²
S. Campana,⁴ S. B. Cenko,^{3,5} N. Gehrels,³ P. Giommi,⁶ C. Gronwall,^{2,7}
F. E. Marshall,³ D. Malesani,⁸ C. B. Markwardt,^{3,9} B. Mingo,¹ J. A. Nousek,²
P. T. O’Brien,¹ J. P. Osborne,¹ C. Pagani,¹ K. L. Page,¹ D. M. Palmer,¹⁰ M. Perri,^{6,11}
J. L. Racusin,³ M. H. Siegel,² B. Sbarufatti^{2,4} and G. Tagliaferri⁴

¹Department of Physics and Astronomy, University of Leicester, Leicester LE1 7RH, UK

²Department of Astronomy and Astrophysics, Pennsylvania State University, 525 Davey Lab, University Park, PA 16802, USA

³NASA Goddard Space Flight Center, Mail Code 661, Greenbelt, MD 20771, USA

⁴INAF, Osservatorio Astronomico di Brera, via E. Bianchi 46, I-23807 Merate, Italy

⁵Joint Space-Science Institute, University of Maryland, College Park, MD 20742, USA

⁶Agenzia Spaziale Italiana (ASI) Science Data Center, I-00133 Roma, Italy

⁷Institute of Gravitation and the Cosmos, Institute for Gravitation and the Cosmos, Pennsylvania State University, University Park, PA 16802, USA

⁸Dark Cosmology Centre, Niels Bohr Institute, University of Copenhagen, Juliane Maries Vej 30, DK-2100 København Ø, Denmark

⁹Department of Astronomy, University of Maryland, College Park, MD 20742, USA

¹⁰Los Alamos National Laboratory, B244, Los Alamos, NM 87545, USA

¹¹INAF–Osservatorio Astronomico di Roma, via Frascati 33, I-00040 Monteporzio Catone, Italy

Accepted 2016 April 4. Received 2016 April 4; in original form 2016 February 15

ABSTRACT

The Advanced Laser Interferometer Gravitational-Wave Observatory (ALIGO) observatory recently reported the first direct detection of gravitational waves (GW) which triggered ALIGO on 2015 September 14. We report on observations taken with the *Swift* satellite two days after the trigger. No new X-ray, optical, UV or hard X-ray sources were detected in our observations, which were focused on nearby galaxies in the GW error region and covered 4.7 deg² (~2 per cent of the probability in the rapidly available GW error region; 0.3 per cent of the probability from the final GW error region, which was produced several months after the trigger). We describe the rapid *Swift* response and automated analysis of the X-ray telescope and UV/Optical telescope data, and note the importance to electromagnetic follow-up of early notification of the progenitor details inferred from GW analysis.

Key words: gravitational waves – methods: data analysis – X-rays: general.

1 INTRODUCTION

The Advanced Laser Interferometer Gravitational-Wave Observatory (ALIGO) observatory [Laser Interferometer Gravitational-Wave Observatory (LIGO) Scientific Collaboration et al. 2015] recently reported the first ever direct detection of gravitational waves (GW; Abbott et al. 2016c), ALIGO event GW150914. One of the most likely sources of GW detectable by ALIGO is the coalescence of a compact binary, i.e. one containing neutron stars (NS) or stellar-mass black holes (BH). Such events may be accompanied by transient electromagnetic (EM) radiation such as a short gamma-ray burst (‘sGRB’; if the binary is viewed close to face-on; see Berger 2014 for a review) or a kilonova (see e.g. Metzger & Berger 2012; Cowperthwaite & Berger 2015). Previous searches for coincident EM and GW emission have produced null results (e.g. Evans et al. 2012; Aasi et al. 2014). In a previous work (Evans et al. 2016;

hereafter ‘Paper I’), we discussed how the *Swift* satellite (Gehrels et al. 2004) could respond to such triggers to search for emission from a short GRB afterglow with the *Swift* X-ray telescope (XRT; Burrows et al. 2005). For GW150914, *Swift* was able to rapidly respond and was the first EM-facility to report results (~15 h after the GW trigger was announced; Evans et al. 2015).

ALIGO uses two approaches to search for GW. The first (burst) searches for GW signals with no prior assumptions about the nature of the signal; the second (compact binary coalescence, or CBC) assumes that the signal comes from the coalescence of a binary comprising NS and/or BH, and uses a template library of expected signals. The ‘Coherent WaveBurst’ (cWB) pipeline, one of the ‘burst’ pipelines, triggered on 2015 September 14 at 09:50:45 UT, reporting a signal with a false alarm rate of 1.178×10^{-8} Hz, i.e. a spurious signal of this significance is expected once every 2.7 yr (this was later revised to less than one every four hundred years; LIGO Scientific Collaboration 2015a and then one per 203 000 yr; Abbott et al. 2016c). This event was announced to the EM follow-up partners on 2015 September 16 at 06:39 UT (Singer 2015). Two skymaps

* E-mail: pae9@leicester.ac.uk

were released originally, one from the cWB pipeline (which uses a likelihood analysis) and a refined skymap from the omicron-LALInferenceBursts (oLIB) pipeline (which uses a Markov-Chain Monte Carlo [MCMC] approach which is more accurate than the cWB approach, but takes longer to perform). For details of these algorithms see Abbott et al. (2016a). We selected the skymap from the latter, known as ‘LIB_skymap’, since the LIGO team reported this as the refined localization (Singer 2015).

The 90 per cent confidence error region in the ‘LIB_skymap’ covered 750 deg². In 2016 January a further analysis was released by the ALIGO team. This was produced from the CBC pipeline, since the event was believed to be a binary coalescence; and yielded the definitive skymap known as ‘LALInference’ LIGO Scientific Collaboration (2015b). This method uses a full MCMC parameter reconstruction. The 90 per cent confidence error region in this map was reduced to 600 deg², LIGO Scientific Collaboration (2015b).

In this Letter, we report on follow-up observations with the XRT and UV/Optical telescope (UVOT; Roming et al. 2005), and we also searched the Burst Alert Telescope (BAT; Barthelmy et al. 2005) data for any sign of hard X-ray emission at the time of the trigger. A summary of all of the EM follow-up of GW150914 was given by the LIGO-EM follow-up team (Abbott et al. 2016b).

Throughout this Letter, errors are quoted at the 90 per cent confidence level unless otherwise stated, and all fluxes and magnitudes are the observed values (i.e. no corrections have been made for reddening or absorption by interstellar/intergalactic gas and dust).

2 SWIFT OBSERVATIONS

Swift contains three instruments. The BAT (Barthelmy et al. 2005) is a coded mask telescope with an energy sensitivity of 15–350 keV and field of view ~ 2 sr. The XRT (Burrows et al. 2005) covers 0.3–10 keV and has a roughly circular field of view with radius 12.35 arcmin. The UVOT has seven filters covering the 1270–6240 Å wavelength range, and a square field of view ~ 17 arcmin to a side. BAT is primarily a trigger instrument not a follow-up instrument and, as discussed in Paper I, the likelihood of a simultaneous BAT+ALIGO trigger is modest. We used both XRT and UVOT to search for a counterpart to the GW event, noting (as per Paper I) that the expected rate of unrelated X-ray transients serendipitously detected is lower than in the optical bands, therefore our strategy is optimized for the XRT.

While Paper I advocated a large-scale rapid tiling with *Swift* in response to a GW trigger, such an operating mode had not been commissioned when ALIGO triggered on GW150914,¹ therefore we were obliged to observe a smaller number of fields. Following Paper I, we convolved the ALIGO sky localization map (we used the ‘LIB_skymap’ which was the best map available at time of our observations; Abbott et al. 2016c) with the Gravitational Wave Galaxy Catalogue (GWGC; White, Daw & Dhillon 2011). We added a 100 kpc halo to each galaxy in the GWGC more than 5 Mpc away,² to reflect possible impact of natal NS kicks. However, unlike our previous work (where pixels in this map had values of 1 or 0) we weighted this map by galaxy luminosity. Each GWGC galaxy was assigned a probability $P = L/L_{\text{tot}}$, where L is the B -band

¹ Indeed, the trigger actually occurred at the end of an engineering run, before the official start of the O1 observing run.

² For galaxies closer than this 5 Mpc, the angular projection of a 100 kpc halo covers an unreasonably large fraction of the sky, but the fraction of binary NS mergers which occur within this distance is negligible: 0.013 per cent assuming they are homogeneously distributed in space and detectable to 100 Mpc by ALIGO.

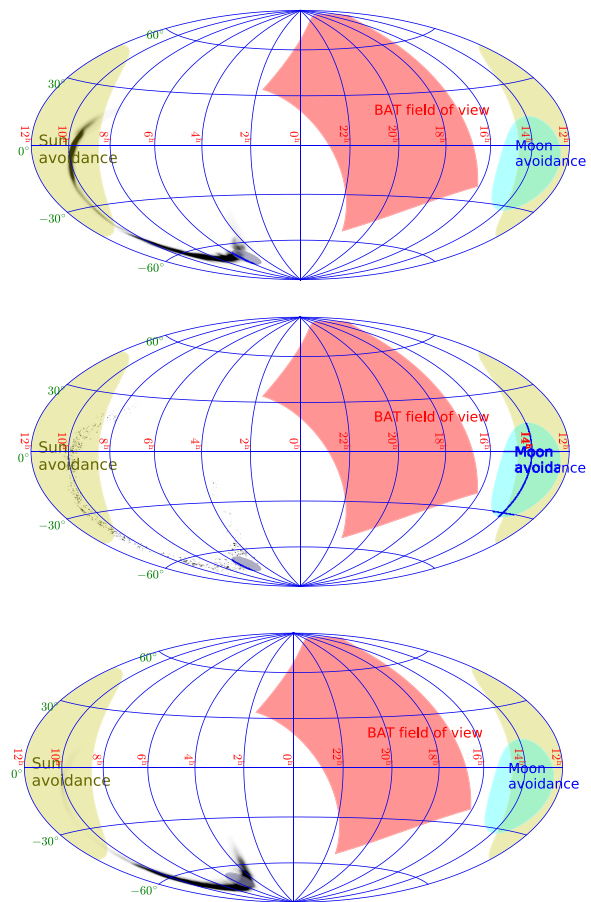


Figure 1. The top two panels show the ‘LIB_skymap’ GW localization map produced by the LIGO-VIRGO consortium (LVC) team on 2015 September 15, in the original form (top) and convolved with our luminosity-weighted GWGC map (middle). The bottom panel shows the revised ‘LALInference’ skymap released on 2016 January 13. Coordinates are equatorial, J2000. The yellow and cyan circles show the regions of the sky which *Swift* could not observe due to the presence of the Sun and Moon, respectively, calculated at the time of the first *Swift* observations. The small, lilac ellipse marks the LMC. The large purple region approximates the BAT field of view at the time of the GW trigger.

luminosity of the galaxy reported in the GWGC and L_{tot} is the total luminosity of all galaxies in the catalogue. This probability was then evenly distributed between all HEALPIX³ pixels corresponding to the galaxy and its halo, i.e. we assumed that the probability of a binary NS merger (which gives rise to the GRB and GW emission) is spatially uniform throughout the host galaxy and its halo.

The LIB_skymap from the ALIGO team and the version convolved with GWGC are shown in Fig. 1, along with the final skymap, released in 2016 January.

Unfortunately a large portion of the error region was within *Swift*’s Sun observing constraint where *Swift*’s narrow field instruments cannot be pointed ($< 47^\circ$ from the Sun). Gehrels et al. (2016) noted that, since most of the galaxy luminosity comes from a small fraction of galaxies, one can opt to only observe the brightest galaxies within the ALIGO error region; Kasliwal et al. (2015) reported a list of such galaxies. Unfortunately, three of their top 10 were within the Sun constraint region. It later transpired that this was less

³ Hierarchical Equal Area isoLatitude Pixelization (Górski et al. 2005), the file format in which ALIGO error regions are disseminated.

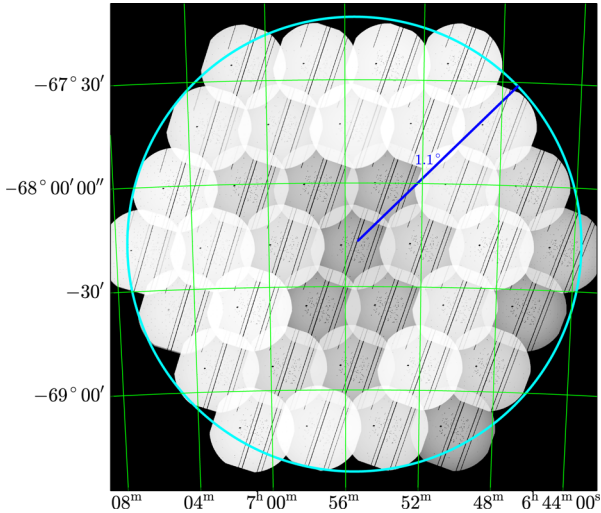


Figure 2. The XRT exposure map of the 37-point tiled observations of the LMC performed with *Swift*, demonstrating the structure of the pattern. The black lines are the vetoed columns on the CCD. The cyan circle has radius of 1.1 and is shown for reference. Axis are RA and Dec., J2000.

of an issue than believed at the time of the GW event, as the probability contained within the Sun constraint region was significantly reduced in the final skymap, as the bottom panel of Fig. 1 shows.

Rather than select where to point the XRT based on individual galaxies, we divided the observable sky into XRT fields of view (since one field may contain multiple galaxies) – circles of radius 12.35 arcmin – and ranked them in decreasing order of probability derived from our GWGC-convolved skymap, and then observed the top five fields from this list, which contained eight GWGC galaxies. Noting that the GW error region also intersected the Large Magellanic Cloud (LMC), we also performed a 37-point tiled observation focused on the LMC (Fig. 2). This tiling formed part of the process of commissioning the ability to observe as Paper I advocated, and as it was the first such test, we were limited to short exposures. A full list of the *Swift* observations is given in Table 1.

3 DATA ANALYSIS

The XRT data analysis was largely automated, using custom software produced by (and running at) the UK *Swift* Science Data Centre at the University of Leicester. This software makes extensive use of the *Swift* software⁴ with the latest CALDB files.⁵

Our baseline source detection system was that developed by Evans et al. (2014) for the *Swift*-XRT Point Source (1SXPS) catalogue. This is an iterative system, that uses a sliding-cell detection method with a background map which is recreated on each pass to account for sources already discovered. The majority of data sets in the 1SXPS catalogue corresponded to a single XRT field of view, and even where multiple fields of view overlapped, images were limited to 1000×1000 pixels ($39.3 \text{ arcmin} \times 39.3 \text{ arcmin}$) in size. For GW150914, we observed a large contiguous region (part of the LMC; Fig. 2) – this region is so large that the background mapping developed for 1SXPS is not properly calibrated, and the coordinates in the tangent-plane projection become inaccurate. We therefore broke the data into ‘analysis blocks’. Each block was no more than 0.55 in radius (equivalent to a 7-point tile), and every

Table 1. *Swift* observations of the error region of GW150914.

Pointing direction (J2000)	Start time ^a (UTC)	Exposure (s)
09 ^h 13 ^m 29 ^s .65, −60°43′37″.4	September 16 at 15:19:27	777
08 ^h 16 ^m 30 ^s .77, −67°38′06″.7	September 16 at 16:54:41	987
07 ^h 28 ^m 42 ^s .38, −66°59′43″.1	September 16 at 18:28:32	970
08 ^h 03 ^m 23 ^s .72, −67°37′17″.2	September 16 at 20:05:37	970
08 ^h 57 ^m 17 ^s .34, −65°26′34″.1	September 16 at 21:42:15	985
LMC observations		
06 ^h 55 ^m 30 ^s .59, −68°18′44″.3	September 17 at 18:26:54	20
06 ^h 59 ^m 13 ^s .43, −68°18′29″.7	September 17 at 18:28:03	42
06 ^h 57 ^m 21 ^s .25, −68°36′12″.8	September 17 at 18:29:12	20
06 ^h 53 ^m 42 ^s .84, −68°36′04″.4	September 17 at 18:30:21	22
06 ^h 51 ^m 53 ^s .97, −68°18′16″.7	September 17 at 18:31:29	32
06 ^h 53 ^m 45 ^s .48, −68°00′43″.4	September 17 at 18:32:38	22
06 ^h 57 ^m 25 ^s .10, −68°01′02″.6	September 17 at 18:33:46	25
07 ^h 01 ^m 1 ^s .84, −68°01′05″.6	September 17 at 18:34:54	35
07 ^h 02 ^m 52 ^s .89, −68°18′56″.6	September 17 at 18:36:02	72
07 ^h 01 ^m 0 ^s .50, −68°36′16″.1	September 17 at 18:37:09	82
06 ^h 59 ^m 11 ^s .14, −68°53′42″.6	September 17 at 18:38:17	37
06 ^h 55 ^m 32 ^s .45, −68°53′32″.4	September 17 at 18:39:25	25
06 ^h 51 ^m 54 ^s .75, −68°53′32″.0	September 17 at 18:40:33	65
06 ^h 50 ^m 5 ^s .28, −68°35′51″.8	September 17 at 18:41:40	52
06 ^h 48 ^m 15 ^s .62, −68°18′20″.6	September 17 at 18:42:47	65
06 ^h 50 ^m 6 ^s .94, −68°00′54″.0	September 17 at 18:43:53	60
06 ^h 51 ^m 56 ^s .98, −67°43′22″.9	September 17 at 18:44:59	67
06 ^h 55 ^m 34 ^s .08, −67°43′36″.1	September 17 at 18:46:04	72
06 ^h 59 ^m 13 ^s .52, −67°43′33″.4	September 17 at 18:47:10	55
07 ^h 02 ^m 51 ^s .97, −67°43′41″.4	September 17 at 18:48:15	62
07 ^h 04 ^m 42 ^s .41, −68°01′15″.1	September 17 at 18:49:21	75
07 ^h 06 ^m 30 ^s .83, −68°18′50″.4	September 17 at 18:50:27	70
07 ^h 04 ^m 41 ^s .09, −68°36′37″.2	September 17 at 18:51:32	60
07 ^h 02 ^m 50 ^s .35, −68°53′43″.9	September 17 at 18:52:38	60
07 ^h 01 ^m 1 ^s .00, −69°11′19″.8	September 17 at 18:53:43	62
06 ^h 57 ^m 21 ^s .83, −69°11′05″.0	September 17 at 18:54:49	67
06 ^h 53 ^m 43 ^s .60, −69°11′06″.9	September 17 at 18:55:55	42
06 ^h 50 ^m 4 ^s .65, −69°11′01″.6	September 17 at 20:02:45	20
06 ^h 48 ^m 14 ^s .61, −68°53′22″.8	September 17 at 20:03:54	32
06 ^h 46 ^m 25 ^s .66, −68°35′44″.9	September 17 at 20:05:02	20
06 ^h 44 ^m 35 ^s .32, −68°18′21″.1	September 17 at 20:06:11	25
06 ^h 46 ^m 27 ^s .88, −68°00′48″.6	September 17 at 20:07:19	35
06 ^h 48 ^m 17 ^s .47, −67°43′23″.8	September 17 at 20:08:27	60
06 ^h 50 ^m 7 ^s .30, −67°25′50″.9	September 17 at 20:09:34	70
06 ^h 53 ^m 44 ^s .83, −67°26′05″.6	September 17 at 20:10:41	77
06 ^h 57 ^m 24 ^s .51, −67°26′04″.1	September 17 at 20:11:48	67
07 ^h 01 ^m 2 ^s .66, −67°26′08″.1	September 17 at 20:12:54	57

^aAll observations were in 2015.

XRT field of view had to be in at least one block. Any redundant blocks (i.e. where every XRT field in the block was also in another block) were removed. Since this meant that some areas of sky were in multiple blocks, we checked for duplicate detections of the same source (based on spatial coincidence) from multiple blocks and merged any that occurred.

In 1SXPS the minimum exposure time permitted was 100 s, however Table 1 shows that many of the observations (those of the LMC) were shorter than this. This is not likely to be a problem regarding spurious source detections; Evans et al. (2014) found that at short exposure times there are very few spurious sources due to the lack of background events. However, this lack of background may mean that we can reduce the signal-to-noise ratio (S/N) threshold for sources to be accepted in short exposure. We simulated 50 s exposure images (both single fields, and 7-point tiles, to represent the extreme sizes of the analysis blocks) in a manner analogous to

⁴ V4.3, part of HEASOFT 6.15.1.

⁵ Released on 2015 July 21.

Table 2. Sources detected by *Swift*-XRT in follow-up of GW150914, with *u*-band magnitudes from UVOT.

RA (J2000)	Dec. (J2000)	Error (90 per cent conf.)	Flux (0.3–10 keV, erg cm ⁻² s ⁻¹)	<i>u</i> Magnitude (AB mag)	Catalogued name
09 ^h 14 ^m 06 ^s .54	−60°32′07″.7	4.8 arcsec	$(1.9 \pm 0.5) \times 10^{-12}$	N/A	XMMSL1 J091406.5-603212
09 ^h 13 ^m 30 ^s .24	−60°47′18″.1	6.1 arcsec	$(5.3 \pm 2.0) \times 10^{-13}$	15.44 ± 0.02^a	ESO 126-2 = 1RXS J091330.1-604707
08 ^h 17 ^m 60 ^s .62	−67°44′03″.9	4.7 arcsec	$(8.9 \pm 2.4) \times 10^{-13}$	17.53 ± 0.05	1RXS J081731.6-674414

^aMagnitude of the core. The galaxy as a whole (removing foreground stars) has a *u* magnitude of 14.15 ± 0.02 .

Evans et al. (2014) and found that for an S/N threshold of 1.3, the rate of spurious detections was $<3/1000$, equivalent to the ‘Good’ flag in 1SXPS; this was therefore used for the short (<100 s) observations.

As discussed in Paper I, the discovery of an X-ray source alone does not identify it as the counterpart to the GW trigger. We therefore gave each detected source a ‘rank’ indicating how likely it is to be related to the GW event, from 1 (very likely) to 4 (very unlikely). This involved comparing our source detections with the *ROSAT* All Sky Survey (RASS; Voges et al. 1999). To do this, we assumed a typical active galactic nucleus (AGN) spectrum, a power law with hydrogen column density $N_{\text{H}} = 3 \times 10^{20}$ cm⁻² and a photon index of $\Gamma = 1.7$. These ranks were defined as follows.

Rank 1: Good GW counterpart candidate. Sources which lie within 200 kpc of a GWGC galaxy, and are either uncatalogued and brighter than the 3σ catalogue limit, or catalogued but brighter than their catalogued flux. In both cases, ‘brighter than’ means that the measured and historical values (or upper limits) disagree at the 5σ level. For uncatalogued sources, the comparison is to the RASS, or to 1SXPS or the *XMM–Newton* catalogues, if an upper limit from those catalogues is available and deeper than the RASS limit.

Rank 2: Possible counterpart. The criteria for this are similar to those above, except that ‘brighter’ is determined at the 3σ level, and there is no requirement for the source to be near a known galaxy.

Rank 3: Undistinguished source. Sources which are uncatalogued, but are fainter than existing catalogue limits, or consistent with those limits at the 3σ level. i.e. sources which cannot be distinguished from field sources.

Rank 4: Not a counterpart. Sources which are catalogued, and which have fluxes consistent with (at the 3σ level) or fainter than their catalogued values.

The relatively conservative flux requirements of rank 1 arise because of biases which cause us to overestimate the ratio between the observed flux and historical flux or limit. The Eddington bias (Eddington 1940) results in the fluxes of sources close to the detection limit being overestimated; this was discussed and quantified for *Swift*-XRT by Evans et al. (2014, section 6.2.1 and figs 9–10). Also, *ROSAT* had a much softer response than *Swift* (0.1–2.4 keV compared to 0.3–10 keV); for sources with harder spectra than in our assumed model (especially those more heavily absorbed) this means that *ROSAT* was less sensitive, i.e. our calculated XRT/*ROSAT* ratio will be too low.

As well as the checks performed to automatically rank each XRT source, the 2MASS catalogue (Skrutskie et al. 2006) and SIMBAD data base (Wenger et al. 2000) were automatically searched, and any sources within the 3σ XRT error region were identified. This information was not used to determine the source rank, but to inform human decisions as to the nature of the source. It is important to note that this spatial correlation does not necessarily mean that the XRT source and the 2MASS/SIMBAD object are the same thing: Evans et al. (2014) showed that ~ 11 per cent of XRT sources with SIMBAD matches, and ~ 64 per cent of those with 2MASS matches are not related but chance alignments.

An automated pipeline was built to search for candidate counterparts in the UVOT observations using standard *HEASOFT* analysis

tools. In the pipeline the tool *UVOTDETECT* was used to search for sources in the sky image files. For each observation searches were made using the longest exposure and the sum of all images if the summed exposure was significantly longer than the longest exposure. Candidate sources whose images were not star-like or were too close to other sources were rejected. Sources without counterparts in the USNO-B1.0 catalogue (Monet et al. 2003) or Hubble Guide Star Catalog (Lasker et al. 2008) were considered possible candidates. The UVOT image near each of these possible candidates was then visually compared with the corresponding region in the Digitized Sky Survey (DSS). This visual comparison was used to reject candidates due to readout streaks or ghost images of bright sources.

The UVOT images near Rank 1 or Rank 2 XRT sources were also examined and compared with the DSS. UVOT source magnitudes or upper limits were determined using the tool *UVOTSOURCE*.

4 RESULTS

Three X-ray objects were found in the initial observations (the five most probable XRT fields, Section 2) and announced by Evans et al. (2015). These were all known X-ray emitters showing no sign of outburst and assigned a rank of 4, see Table 2 for details. XMMSL1 J091406.5-603212 was automatically flagged as being potentially spurious due to optical loading as it is spatially coincident with HD 79905 which SIMBAD reports as a B9.5 star (Houk & Cowley 1975) with a V magnitude of 7.436 (Kiraga 2012), above the threshold where optical loading is likely to affect the X-ray measurements.⁶ The measured count rate (0.045 ± 0.011 ct s⁻¹) is however slightly lower than that in the RASS (0.10 ± 0.01 ct s⁻¹ when converted to an XRT-equivalent rate using the AGN spectrum introduced above), suggesting that the optical loading has not resulted in a spurious X-ray detection. No other SIMBAD objects match the position of this source. ESO126-2 is listed as an AGN by SIMBAD, whereas 1RXS J081731.6-674414 is simply listed as an X-ray source.

The 3σ upper limit on any other X-ray point source in the initial five fields is 1.5×10^{-2} ct s⁻¹, which corresponds to a flux of 6.5×10^{-13} erg cm⁻² s⁻¹, assuming the AGN spectrum defined above. For the LMC observations the typical upper limit was 0.16 ct s⁻¹, or 6.9×10^{-12} erg cm⁻² s⁻¹, corresponding to a luminosity of 2.0×10^{36} erg s⁻¹.

UVOT observations were all carried out in the *u* filter, two of the sources were detected and one lay outside the UVOT field of view. Details are in Table 2. No transient sources were detected by UVOT down to an AB magnitude of ~ 19.8 for the initial five galaxies, and 18.8 for the LMC.

Both the rapidly available ALIGO sky localization and the later, revised version had no probability within *Swift*-BAT’s nominal field of view, therefore the lack of a simultaneous trigger from BAT is not informative. However, BAT can detect GRBs from outside of the field of view, by means of gamma-rays that leak through the

⁶ http://www.swift.ac.uk/analysis/xrt/optical_tool.php

sidewall shielding. A search for any corresponding rate increases from a correlated GRB within ± 100 s of the GW signal found no peaks above the 3σ value of 200 ct s^{-1} above background in the nominal 50–300 keV energy range at a 1 s time-scale. To convert this to a flux limit requires precise knowledge of the direction in which the event occurred which we do not have for GW 150914.

Fermi-GBM reported a possible low significance gamma-ray event temporally coincident with the ALIGO trigger (Blackburn et al. 2015; Connaughton et al. 2016), although this was not detected by *INTEGRAL* (Ferrigno et al. 2015) and no signal was seen in BAT either. The best position deduced by Connaughton et al. (2016) was below the Earth limb from the perspective of BAT, so the lack of signal is perhaps not surprising; however the GBM localization is very poor, covering thousands of square degrees. As just noted, this prevented us from creating an accurate flux limit for BAT; however, considering the range of possible angles, an approximate 5σ upper limit over the 14–195 keV band is $\sim 2.4 \times 10^{-6} \text{ erg cm}^{-2} \text{ s}^{-1}$. Connaughton et al. (2016) fit the spectrum of the GBM event as a power law with a photon index of 1.4; the fluence from this spectrum was $2.4_{-1.0}^{+1.7} \times 10^{-7} \text{ erg cm}^{-2}$. Since the duration of the pulse was 1 s, the flux has the same numeric value. This spectrum gives a flux of $7.63 \times 10^{-8} \text{ erg cm}^{-2} \text{ s}^{-1}$; below the upper limit derived from BAT. Therefore even if the GBM detection was a real astrophysical event, it was likely too faint for BAT to have detected, given that the source was outside the coded field of view.

5 DISCUSSION AND CONCLUSIONS

The XRT observations covered 4.7 deg^2 , and contained 2 per cent of the probability from the original ‘LIB_skymap’ ALIGO error region (8 per cent if this is convolved with the GWGC), and were obtained from 53.5 to 82.3 h after the GW trigger. However, Abbott et al. (2016c) reported that the most likely source of the GW event is a binary BH trigger at 500 Mpc. Since the GWGC only extends to 100 Mpc and the coalescence of two stellar mass BHs is not expected to produce EM radiation, our lack of detection is not surprising. Additionally, the recently released revised skymap ‘LALInference’ contains much less probability at the location of the XRT fields, with those field containing only 0.3 per cent of the GW probability (this figure does not change with galaxy convolution).

The possible detection of an sGRB coincident with the ALIGO trigger reported by *Fermi*-GBM is intriguing, but unfortunately we are not able to place any meaningful constraints on its brightness with the BAT. None of the GW probability was within the BAT field of view, and the flux limits we can derive for emission received through the sidewalls of the instrument are above the level expected from the GBM data.

Although the *Swift* observations did not yield the detection of an EM counterpart to the GW trigger, we have demonstrated that *Swift* is able to respond very rapidly to GW triggers with *Swift*: the three X-ray sources we detected were reported to the GW-EM community within 15 h of the trigger being announced. In the event of a nearby binary NS merger triggering ALIGO, such rapid response, analysis and dissemination will be vital. It is also evident that the decisions made regarding where to observe with *Swift* are best informed if details such as estimated distances and masses are available rapidly from the GW teams, as noted by the GW-EM summary paper (Abbott et al. 2016b), and it is expected that the latencies in deriving these parameters will be reduced in the future. We have also commissioned new observing modes with *Swift* which will allow us to perform much more extensive follow-up observations of future GW triggers.

ACKNOWLEDGEMENTS

This work made use of data supplied by the UK Swift Science Data Centre at the University of Leicester, and used the ALICE High Performance Computing Facility at the University of Leicester. This research has made use of the XRT Data Analysis Software (XRT-DAS) developed under the responsibility of the ASI Science Data Center (ASDC), Italy. PAE, APB, BM, KLP and JPO acknowledge UK Space Agency support. SC and GT acknowledge Italian Space Agency support. This publication makes use of data products from the Two Micron All Sky Survey, which is a joint project of the University of Massachusetts and the Infrared Processing and Analysis Center/California Institute of Technology, funded by the National Aeronautics and Space Administration and the National Science Foundation, and the SIMBAD data base, operated at CDS, Strasbourg, France. Fig. 1 was created using the KAPETYN package (Terlouw & Vogelaar 2015). We thank the anonymous referee for their helpful feedback on the original version of the Letter.

REFERENCES

- Aasi J. et al., 2014, *Phys. Rev. D*, 89, 122004
 Abbott B. P. et al., 2016a, preprint (arXiv:1602.03843)
 Abbott B. P. et al., 2016b, preprint (arXiv:1602.08492)
 Abbott B. P. et al., 2016c, *Phys. Rev. Lett.*, 116, 061102
 Barthelmy S. D. et al., 2005, *Space Sci. Rev.*, 120, 143
 Berger E., 2014, *ARA&A*, 52, 43
 Blackburn L. et al., 2015, *GCN Circ.*, 18339
 Burrows D. N. et al., 2005, *Space Sci. Rev.*, 120, 165
 Connaughton V. et al., 2016, preprint (arXiv:1602.03920)
 Cowperthwaite P. S., Berger E., 2015, *ApJ*, 814, 25
 Eddington Sir A. S., 1940, *MNRAS*, 100, 354
 Evans P. A. et al., 2012, *ApJS*, 203, 28
 Evans P. A. et al., 2014, *ApJS*, 210, 8
 Evans P. A. et al., 2015, *GCN Circ.*, 18331
 Evans P. A. et al., 2016, *MNRAS*, 455, 1522 (Paper I)
 Ferrigno C., Savchenko V., Mereghetti S., Kuulkers E., Bazzano A., Bozzo E., Courvosier T. J.-L., 2015, *GCN Circ.*, 18354
 Gehrels N. et al., 2004, *ApJ*, 611, 1005
 Gehrels N., Cannizzo J. K., Kanner J., Kasliwal M. M., Nissanke S., Singer L. P., 2016, *ApJ*, 820, 136
 Górski K. M., Hivon E., Banday A. J., Wandelt B. D., Hansen F. K., Reinecke M., Bartelmann M., 2005, *ApJ*, 622, 759
 Houk N., Cowley A. P., 1975, University of Michigan Catalogue of two-dimensional spectral types for the HD stars, Volume I. Declinations -90_ to -53_f0.
 Kasliwal M. M., Cannizzo J. K., Gehrels N., Evans P., 2015, *GCN Circ.*, 18340
 Kiraga M., 2012, *Acta Astron.*, 62, 67
 Lasker B. M. et al., 2008, *AJ*, 136, 735
 LIGO Scientific Collaboration 2015a, *GCN Circ.*, 18851
 LIGO Scientific Collaboration 2015b, *GCN Circ.*, 18858
 LIGO Scientific Collaboration et al., 2015, *Class. Quantum Gravity*, 32, 074001
 Metzger B. D., Berger E., 2012, *ApJ*, 746, 48
 Monet D. G. et al., 2003, *AJ*, 125, 984
 A.Roming P. W. et al., 2005, *Space Sci. Rev.*, 120, 95
 Singer L., 2015, *GCN Circ.*, 18330
 Skrutskie M. F. et al., 2006, *AJ*, 131, 1163
 Terlouw J. P., Vogelaar M. G. R., 2015, Kapteyn Package, version 2.3. Kapteyn Astronomical Institute, Groningen
 Voges W. et al., 1999, *A&A*, 349, 389
 Wenger M. et al., 2000, *A&AS*, 143, 9
 White D. J., Daw E. J., Dhillon V. S., 2011, *Class. Quantum Gravity*, 28, 085016

This paper has been typeset from a $\text{\TeX}/\text{\LaTeX}$ file prepared by the author.